Cerebral Cortex, December 2015;25: 4839–4853

doi: 10.1093/cercor/bhv188
Advance Access Publication Date: 28 August 2015
Original Article

ORIGINAL ARTICLE

Dendritic and Axonal Architecture of Individual Pyramidal Neurons across Layers of Adult Human Neocortex

Hemanth Mohan[1,†], Matthijs B. Verhoog[1,†], Keerthi K. Doreswamy[1], Guy Eyal[2], Romy Aardse[1], Brendan N. Lodder[1], Natalia A. Goriounova[1], Boateng Asamoah[1], A.B. Clementine B. Brakspear[1], Colin Groot[1], Sophie van der Sluis[3], Guilherme Testa-Silva[1], Joshua Obermayer[1], Zimbo S.R.M. Boudewijns[1], Rajeevan T. Narayanan[1], Johannes C. Baayen[4], Idan Segev[2], Huibert D. Mansvelder[1,‡] and Christiaan P.J. de Kock[1,‡]

[1]Department of Integrative Neurophysiology, Center for Neurogenomics and Cognitive Research, VU University Amsterdam, Amsterdam 1081 HV, The Netherlands, [2]Department of Neurobiology and Edmond and Lily Safra Center for Brain Sciences, The Hebrew University of Jerusalem, Jerusalem 91904, Israel, [3]Department of Clinical Genetics, Section Complex Trait Genetics, Center for Neurogenomics and Cognitive Research, VU Medical Center, Amsterdam, The Netherlands, and [4]Department of Neurosurgery, VU University Medical Center, Amsterdam 1081 HV, The Netherlands

Address correspondence to Huibert D. Mansvelder, Email: h.d.mansvelder@vu.nl or Christiaan P.J. de Kock, Email: ckock@falw.vu.nl

[†]Hemanth Mohan and Matthijs B. Verhoog contributed equally to this work.

[‡]Huibert D. Mansvelder and Christiaan P.J. de Kock share senior authorship.

Abstract

The size and shape of dendrites and axons are strong determinants of neuronal information processing. Our knowledge on neuronal structure and function is primarily based on brains of laboratory animals. Whether it translates to human is not known since quantitative data on "full" human neuronal morphologies are lacking. Here, we obtained human brain tissue during resection surgery and reconstructed basal and apical dendrites and axons of individual neurons across all cortical layers in temporal cortex (Brodmann area 21). Importantly, morphologies did not correlate to etiology, disease severity, or disease duration. Next, we show that human L(ayer) 2 and L3 pyramidal neurons have 3-fold larger dendritic length and increased branch complexity with longer segments compared with temporal cortex neurons from macaque and mouse. Unsupervised cluster analysis classified 88% of human L2 and L3 neurons into human-specific clusters distinct from mouse and macaque neurons. Computational modeling of passive electrical properties to assess the functional impact of large dendrites indicates stronger signal attenuation of electrical inputs compared with mouse. We thus provide a quantitative analysis of "full" human

neuron morphologies and present direct evidence that human neurons are not "scaled-up" versions of rodent or macaque neurons, but have unique structural and functional properties.

Introduction

The cellular organization of the human brain has been the focus of neuroscience research ever since Ramon y Cajal and Golgi's groundbreaking work of more than a century ago. From many experimental and computational studies investigating neurons in brains of laboratory animals, we now know that a strong interdependence exists between dendritic and axonal morphology and information processing capabilities of a neuron (Mainen and Sejnowski 1996; Yuste and Tank 1996; Segev and Rall 1998; Magee 2000; van Elburg and van Ooyen 2010; Eyal et al. 2014). Mammalian dendrites have a rich repertoire of electrical and chemical dynamics, and individual neurons are capable of sophisticated information processing (Yuste and Tank 1996). Dendritic geometry strongly affects the action potential firing pattern of neurons (Mainen and Sejnowski 1996). In addition, we recently found that the size of dendritic arbors strongly modulates the shape of the action potential onset at the axon initial segment; it is accelerated in neurons with larger dendritic surface area (Eyal et al. 2014). Action potential onset rapidness is key in determining the capability of the axonal spikes to encode rapid changes in synaptic inputs (Fourcaud-Trocme et al. 2003; Ilin et al. 2013). Hence, neurons with larger dendritic arbors have improved encoding capabilities.

Whether structure and function of neurons in brains of laboratory animals such as rodents accurately reflect human brain organization is only partly known. Techniques commonly used in humans to study brain organization such as EEG, MEG, and MRI lack cellular resolution. Molecular and histological approaches using postmortem human brain material have limitations to unravel extensive subcellular architecture, since typically, only partial cellular morphologies can be resolved and quantitative analysis is performed on subcompartments of the apical/basal dendritic tree (Braak 1980; Ong and Garey 1990; Elston et al. 2001; Jacobs et al. 2001; Anderson et al. 2009; Petanjek et al. 2011; Rosoklija et al. 2014). Additionally, postmortem delays to brain tissue fixation may effect morphology of fine cellular structures (de Ruiter and Uylings 1987; Swaab and Uylings 1988; Oberheim et al. 2009). Still, multiple studies provide evidence that the cellular organization of the human cortex may differ substantially from that of laboratory animals (Nimchinsky et al. 1999; Elston et al. 2001; Rakic 2009; Clowry et al. 2010; Bianchi et al. 2013; Geschwind and Rakic 2013; Hladnik et al. 2014; Luebke et al. 2015). First, astrocytes in human temporal cortex are 2–3 times larger and processes are 10 times more complex than their rodent counterparts (Oberheim et al. 2009); second, interneurons are more numerous and diverse in human (Dzaja et al. 2014; Radonjic et al. 2014); third, absolute numbers for neurons, spines, and synapses are highly species-specific and finally, density values for neurons, spines, and synapses are also highly species-specific (DeFelipe et al. 2002; DeFelipe 2011). In a comparison between single subjects, basal dendrites of pyramidal neurons in human prefrontal cortex of a 48-year-old subject were more branched and contained more spines than those in the prefrontal cortex of a 10-year-old macaque and an 18-month-old marmoset monkey (Elston et al. 2001). Comprehensive and quantitative datasets on full human neuronal morphologies including basal dendrites, apical dendrites (with oblique dendrites and distal tuft), and axonal architecture are however lacking. As a consequence, it has never been tested directly whether neocortical pyramidal neurons in human brain show a larger dendritic structure of both apical and basal dendrites. We addressed this gap in our understanding of human brain organization using intracellular dye loading of individual excitatory neurons in acute, living brain slices of human temporal cortex to avoid potential effects of postmortem delays on cellular morphology. The dimensions of our living brain slices (350 µm) exceed typical slice dimensions for conventional Golgi-Cox stainings on human brain samples (100–200 µm, (Jacobs et al. 2001; Petanjek et al. 2008; Zeba et al. 2008)) and truncation artifacts due to sectioning are therefore relatively small (van Pelt et al. 2014). Using this approach, we tested the hypothesis that total dendritic length of human Layer (L)2 and L3 pyramidal neurons (including basal, apical oblique dendrites, main apical trunk, and distal tuft) are distinct from mouse and macaque pyramidal neurons. We find that the majority of the human temporal cortex pyramidal neurons clustered as a separate class distinct from both mouse and macaque temporal cortex pyramidal neurons. These findings show that human pyramidal neurons differ in their subcellular architecture and suggest that human pyramidal neurons have information processing capabilities distinct from rodent and macaque neurons.

Materials and Methods

Human Brain Slice Preparation

All procedures on human tissue were performed with the approval of the Medical Ethical Committee of the VU University Medical Centre, written consent by patients involved, and in accordance with Dutch license procedures and the declaration of Helsinki. Human brain resection material that had to be removed for the surgical treatment of deeper brain structures typically originated from gyrus temporalis medium (Brodmann area 21, occasionally gyrus temp. inferior or gyrus temp. superior), 2–6 cm posterior with respect to the temporal pole (human-specific speech areas were avoided during resection surgery through functional mapping). We obtained neocortical tissue from 28 patients (16 females, 12 males; age range, 19–66 years) predominantly treated for mesial temporal sclerosis (16 cases), for the removal of a hippocampal tumor (7 cases), epilepsy due to meningitis (2 cases), or cavernoma (3 cases). In all patients, the resected neocortical tissue was located outside the epileptic focus or tumor and displayed no structural/functional abnormalities in preoperative MRI investigations. Upon surgical resection, the cortical tissue block (several cm^3s) was instantaneously transferred to ice-cold artificial cerebral spinal fluid containing (in mM): 110 choline chloride, 26 $NaHCO_3$, 10 D-glucose, 11.6 sodium ascorbate, 7 $MgCl_2$, 3.1 sodium pyruvate, 2.5 KCl, 1.25 NaH_2PO_4, and 0.5 $CaCl_2$ and transported to the neurophysiology laboratory, which is located within a few hundred meters of the operating room. Transition time between resection of tissue and slice preparation was typically <10 min. Next, the tissue block was stripped from potential traumatic edges and the pia-white matter (WM) axis identified. Then, the tissue block was stabilized on a platform and 350-µm brain slices were prepared on a vibratome slicer as described before (Testa-Silva et al. 2010; Verhoog et al. 2013). Only completely intact, undamaged slices in which cortical

layers span from pia to WM were selected for electrophysiology, stored for 30 min at 34°C and subsequently left to recover for at least 1 h at room temperature before recording in artificial cerebrospinal fluid (aCSF) containing (in mM): 125 NaCl, 3 KCl, 1.25 NaH_2PO_4, 1 $MgSO_4$, 2 $CaCl_2$, 26 $NaHCO_3$, and 10 glucose. All aCSF and slicing solutions were continuously bubbled with carbogen gas (95% O_2, 5% CO_2) and had an osmolarity of 300 mOsm. Slices in the recording chamber were submerged in aCSF (32–35°C) and whole-cell patch-clamp recordings were made with Multiclamp 700A/B amplifiers (Molecular Devices) using standard borosilicate glass pipettes (3.5–5.5 MΩ resistance) filled with intracellular solution containing (in mM): 110 K-gluconate; 10 KCl; 10 HEPES; 10 K_2phosphocreatine; 4 ATP-Mg; 0.4 GTP, pH adjusted with KOH to 7.3 (290–300 mOsm). Intracellular solution was supplemented with biocytin (5 mg/mL) to ensure dye labeling of neurons in parallel to electrophysiology. Slices or individual neurons of human cortical tissue showed no sign of spontaneous epileptiform activity. After recordings, slices were fixed in 4% paraformaldehyde and the recorded cells were revealed with the chromogen 3,3-diaminobenzidine tetrahydrochloride using the avidin–biotin–peroxidase method (Horikawa and Armstrong 1988). Slices were mounted on slides and embedded in mowiol (Clariant GmbH, Frankfurt am Main, Germany). Neurons without apparent slicing artifacts were reconstructed using Neurolucida software (Microbrightfield, Williston, VT, USA), using a ×100 oil objective. To determine shrinkage due to tissue fixation, staining, and mounting (Egger et al. 2008), the post-mounting thickness of a subset of 10 human and mouse slices was measured, but no statistical difference was observed (140.7 vs. 137.8 µm, medians for human and mouse, $P > 0.05$, Mann–Whitney). Considering original slice thickness during in vitro electrophysiology (350 µm), shrinkage in the z-plane is 63 ± 10% (see also (Egger et al. 2008)). Shrinkage correction of reconstructed morphologies and subsequent quantification of the total dendritic length (TDL) reveals that TDL increases only by 11 ± 2% after shrinkage correction ($n = 5$ examples) suggesting that most dendritic structures in our digital reconstructions consist of branches traveling in the *xy* plane.

We compared our reconstructions of human and mouse pyramidal neurons (see below) with pyramidal neuron morphologies of Macaque *fascicularis* and Macaque *mulatta*. These morphologies were selected based on labeling method (intracellular dye injection) and reconstruction quality (400-µm sections were used and distal dendrites included in reconstruction) and files downloaded from Neuromorpho.org (cell IDs *M. fascicularis*: cnic_019–024 and cnic_055–060, *M. mulatta:* cnic_007–012 and cncic_050–054 (Duan et al. 2003)). These morphologies also suffered from shrinkage due to histological processing (Duan et al. 2003), but quantitative analysis was performed without shrinkage correction. It is important to note therefore, that all measurements underrepresent in vivo-like dendritic and axonal measures.

Nissl Staining

Slices were rinsed in Na-acetate buffer (0.5442% NaOAc and 0.9608% acetic acid) and incubated for 10–15 min in 0.5% Cresyl-violet. Immediately after Cresyl-violet staining, slices were coverslipped and images were taken at ×4 magnification.

Mouse Brain Slice Preparation

C57Bl/6J mice (7–15 weeks) were decapitated and brains submerged in ice-cold aCSF. Coronal sections (350 µm) including temporal association cortex (TEa, coordinates relative to Bregma: –4.16 mm posterior, 3.85 mm lateral) were cut on a vibratome. The same methodology was used for human and mouse samples, including electrophysiological recordings, biocytin filling, histological processing, and reconstruction methods. For solutions and detailed recording procedures, see "human brain slice preparation" section.

Hierarchical Agglomerative Clustering

Dendrograms were constructed using statistics toolbox in Matlab (Mathworks, Natick, MA, USA). Since the number of branch points and total dendritic length were correlated (Fig. 6F), only TDL was used for clustering. Neurons were clustered based on the Euclidean distance between their TDL and number of clusters determined by Thorndike procedure (Thorndike 1953). The dendrograms were validated using their cophenetic correlation coefficient.

Statistical Analysis of Segment Length in Apical Tuft, Apical Obliques, and Basal Dendrites

To compare change in segment length as a function of distance from the soma between human and mouse apical oblique, tuft and basal dendrites, we fitted a multilevel model (MLM, (Hox 2010)) using the Mixed Models procedure in IBM SPSS Statistics 21 (IBM Corporation, Armonk, NY, USA). MLM can handle the fact that not all cells have the same number of dendritic segments, and that each cell can yield multiple measurements of segments of the same order. In addition, MLM allows the estimation of random effects, that is, individual differences in the length of the first segment, and in the rate of increase (Aarts et al. 2014). In our analyses, both linear and quadratic terms were included to model the change in segment length as a function of the order of the segments.

Detailed Compartment Models of Mouse and Human Pyramidal Neurons

The electrotonic dendrograms in Figure 8*B1*,*B2* were constructed using the trees toolbox (Cuntz et al. 2010), whereas the compartmental modeling simulations of 3D reconstructed neurons shown in Figure 8*C1–E2* were performed using NEURON 7.2 (Carnevale and Hines 2006).

Results

Human brain organization at subcellular level is typically studied in postmortem brain material obtained from autopsy surgery. The postmortem delay in these cases is typically 23–26 h (Ong and Garey 1990; Jacobs et al. 1997, 2001), although optimization protocols have been developed to limit autolysis time and ensure tissue fixation within 2–3 h (de Ruiter and Uylings 1987; Ravid and Swaab 1993; Elston et al. 2001; Morales et al. 2014). However, even under these conditions, structural changes as a consequence of fixation delay cannot be excluded. To be able to digitally reconstruct in vivo-like apical dendrites, basal dendrites as well as axons belonging to the same neuron, we filled single neurons by dye loading during whole-cell patch-clamp recordings from individual human cortical neurons in living brain tissue (Verhoog et al. 2013; Eyal et al. 2014; Testa-Silva et al. 2014). Brain tissue was obtained from patients with drug-resistant epileptic seizures associated with different, unrelated brain pathologies such as mesiotemporal sclerosis (MTS), subcortical tumors, cavernoma, meningitis, or subcortical lesions ($n = 28$ patients, age range 19–66 years, Table 1). Disease history in our patient cohort

showed a wide range in epilepsy-related parameters such as years since epilepsy onset, seizure frequency, or presurgery medication. Importantly however, only neocortical brain tissue was used that was not part of the disease, but which had to be removed to gain access to deeper brain structures for surgical treatment.

To enable classification and registration of single neuron morphologies to a standard structural reference frame, we performed Nissl staining on 50-µm sections to reveal layer borders in human temporal cortex (Fig. 1*A*,*B*). First, a sharp increase in cell body densities was observed at 252 ± 7 µm from pia delineating the border between L(ayer) 1 and 2 (Fig. 1*A*,*C*, $n = 5$). Second, increased cell densities (but smaller cell bodies) were encountered from 1201 ± 186 to 1582 ± 220 µm, indicative of L4 (Fig. 1*A*,*C*). Finally, the border delineating the WM was located at 2772 ± 359 µm (Fig. 1*A*,*C*). This is in line with previous studies that characterized the anatomical and cytoarchitectural structure of the human temporal cortex (Ong and Garey 1990; Fischl and Dale 2000; DeFelipe et al. 2002; DeFelipe 2011).

Intracellular recordings for biocytin loading were targeted to pyramidal shaped cell bodies (Fig. 1*D*–*F*) identified by infrared differential interference contrast microscopy. Our data are therefore biased to pyramidal neurons and prevent quantification of relative occurrence of other reported morphologies. Of >500 biocytin-filled neurons, 91 neurons across all layers of human temporal cortex were selected for 3D dendritic reconstruction (Fig. 2). To include a neuron for reconstruction, first the biocytin signal had to be dense and uniform throughout distal dendrites. Second, dendritic structures had to show minor cutting artifacts by the slicing procedure and had to be retained in the slice as much as can be expected realistically. These 2 criteria rejected about 80% of recovered neurons from reconstruction, mainly because of obvious truncation of the apical dendrite. After reconstruction, morphologies were checked for accurate reconstruction in x/y/z planes, dendritic diameter, and no unconnected dendrites. Finally, reconstructions were crosschecked for false-positive/false-negative dendrites using an overlay in Adobe Illustrator between the Neurolucida reconstruction and Z-stack projection image from Surveyor Software (Chromaphor, Oberhausen, Germany).

Reconstructed neurons were exclusively spiny, indicative of excitatory nature and were categorized according to pia-soma distance (Fig. 2). At cortical depths corresponding to L2–L3 in the Nissl stainings (Fig. 1), neurons were encountered with multiple basal dendrites and one apical dendrite projecting towards the pial surface. In superficial L2 and L3, a depth-dependent gradual increase in both basal and apical dendrite length was observed, accompanied by an increase in # of branch points (Fig. 3*A*–*E*). At the L3–L4 border, a sharp decline in TDL was observed for individual neurons due to stellate-like morphologies from which an extensive apical dendrite was missing (Figs 2 and 3*A*–*D*). This was not the result of a slice-cutting artifact; dendrites of these neurons were complete within the slice. Deeper

Table 1 Patient parameters

Gender	Age (years)	Age at epilepsy onset (years)	Diagnosis	Seizure frequency (per month)	Antiepileptic drugs (presurgery)	Reconstructed neurons (#)
M	41	6	Cavernoma	2	CBZ	4
F	20	11	MTS	32	LEV, VPA	2
F	66	63	Tumor	0.25	no AE drugs	5
F	31	16	Tumor	12	CBZ, LEV	2
M	39	33	MTS	32	CBZ	3
F	58	46	MTS	1	CZP	1
M	28	24	Tumor	30	KEP, LAM	6
F	29	13	MTS	32	LTG, TPM	4
M	21	16	Tumor	2	CBZ, LEV	2
F	27	14	MTS	120	CBZ, LTG	8
M	41	10	Tumor	28	CBZ, LTG	8
F	23	15	MTS	9	LEV, OXC	1
F	53	6	MTS	10	CBZ, CLB	2
M	19	17	MTS (meningitis)	450	CLB, OXC	2
F	31	10	MTS	6	LEV, LAM	2
F	40	24	MTS	30	CBZ, FRI	1
F	31	7	MTS	88	FRI, CBZ, VGB	1
F	35	1	MTS	0.7	CZP, LCS, LTG, LEV	1
M	54	45	Cavernoma	30	VPA	1
M	25	9	MTS	2	CLB, LCS, LEV	5
F	31	21	MTS	4	CBZ, CLB	1
M	49	8	MTS	2	CBZ, CLB, LEV	4
M	25	24	Tumor	8	LEV, CBZ, LCS	6
F	45	23	MTS (meningitis)	3	CBZ, CLB, LTG	10
F	47	26	Tumor	8	CBZ	2
F	30	2	Cavernoma	9	CLB, OXC	1
M	44	4	MTS	8	LTG, LEV	3
M	25	15	MTS	8	LEV	3

Note: Patient-specific disease history and number of reconstructed neurons for individual patients.
CBZ, carbamazepine; CZP, clonazepam; KEP, keppra; LAM, lamictal; LEV, levetiracetam; LTG, lamotrigine; LCS, lacosamide; OXC, oxcarbazepine; TPM, topiramate; VPA, sodium valproate.

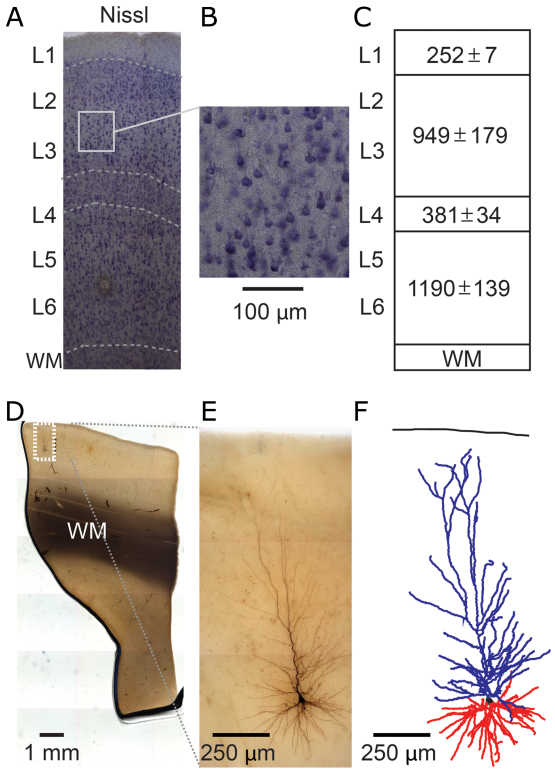

Figure 1. 3D reconstruction of single-cell dendritic morphology in human temporal cortex. (*A*,*B*) Nissl staining to reveal layer boundaries (WM, white matter; L, layer). (*C*) Cortical layer dimensions (in µm ± standard deviation, $n = 5$). (*D*) Low-magnification view of biocytin-filled neuron. (*E*) High-magnification view of same neuron in *D*. (*F*) Example 3D dendritic reconstruction of neuron shown in *D* and *E*. Apical dendrite in blue, basal dendrites in red.

layers (L5 and L6) were characterized by relatively heterogeneous morphologies including shorter basal dendrites and irregularly shaped apical dendrites (Figs 2 and 3*A*–*D*). The gradual, depth-dependent increase in morphological complexity in superficial layers was also reflected in Sholl analysis, in addition to the general drop for neurons in L4–L6 (Fig. 3*F*,*G*).

Compared with standardization of laboratory animal experiments, it is not possible to reach the same standards for human brain research. Since patient history may influence neuronal morphology, we tested whether patient-related parameters at the time of resection surgery or disease history correlate to morphological parameters such as TDL and number of branch points. We first determined the median TDL and # of branch points for individual subjects, and these $n = 28$ median values were used to determine correlations to patient-specific parameters. First, we found that both TDL and number of branch points were not significantly correlated to age (Fig. 4*A*,*B*). Somapia depth (layer location) versus age was also not correlated (ρ 0.17, Spearman $P = 0.11$), indicating unbiased sampling across layers versus age. Next, we determined whether disease history (years between epilepsy onset and age at resection surgery) correlated to TDL and/or number of branch points, but did not find a significant relationship (Fig. 4*C*,*D*). Seizure frequency (number of seizures per month) did also not correlate to TDL and number of branch points (Fig. 4*E*,*F*). Finally, even when we approximate the total number of seizures (years of epilepsy × number of seizures/year), we did not find a correlation for both TDL and number of branch points (data not shown, TDL $\rho = -0.02$, $P = 0.90$, # of branch points $\rho = -0.07$, $P = 0.72$). Thus, we did not find any significant correlation between disease history and morphological parameters within our patient sample. Additionally, morphological parameters directly tested between the 2 patient groups (MTS versus tumor/cavernoma/meningitis) did not reveal consistent differences ($P = 0.28$ for TDL, $P = 0.81$ for # of branch points, Wilcoxon rank sum test), and single-cell data were therefore pooled.

In vivo approaches to reconstruct single neuron axonal morphology generate axonal trees than can be an order of magnitude larger compared with in vitro approaches on the same neuronal population (Bruno et al. 2009; Oberlaender et al. 2011; Narayanan et al. 2015). Since axonal morphologies have not been obtained for human neurons before and in vivo approaches are not available for individual human neurons, we reconstructed in vitro axons of 20 human neurons sampled across all layers of medial temporal cortex (Fig. 5*A*). We quantified the depth dependence of polarity of axonal arborizations (Fig. 5*B*,*C*, quantified as max/mean for 36 different directions), total axon length (Fig. 5*D*), and number of branch points (Fig. 5*E*,*F*). We found that direction selectivity of axonal projections increased with somatic depth (Fig. 5*C*), but not axonal length (Fig. 5*D*) or number of branch points (Fig. 5*E*), suggesting that only polarization of axonal projections depends on neuron location (for instance cell #17). Total axonal length versus number of branch points was also significantly correlated (Fig. 5*F*).

Our results may suggest layer-specific axonal architecture and may reflect a trend towards columnar organization in deeper layers, at least at short intracortical distances. Axonal reconstructions of human neurons in combination with information on dendritic architecture, dendritic spine, and axonal bouton densities in our view will be highly instrumental for any attempt to "reverse engineer" the human cortical column. However, organizational principles of axons will need to be confirmed by single axon reconstructions in larger pieces of human cortical tissue in the future.

To directly compare the size and complexity of dendritic arborization across species, we reconstructed pyramidal neurons from superficial L2 and L3 of adult mouse temporal cortex using the exact same methodology for slice preparation, dye loading, histological processing, and neuronal reconstruction as for the human neurons. We used L2 and L3 pyramidal neurons at comparable cortical depths with respect to the pia-WM span ($n = 15$, age 7–15 weeks, Fig. 6*A*,*B*). In addition, we used previously published complete dendritic morphologies from *Macaca fascicularis* (crab-eating macaque) and *Macaca mulatta* (rhesus monkey) L2 and L3 temporal cortex (Neuromorpho.org; Duan et al. 2002, 2003; Ascoli 2006). Only pyramidal neurons from L2 and L3 temporal cortex were used to compare pyramidal neurons from human, mouse, *M. fascicularis* and *M. mulatta*. Total dendritic length (TDL) was 3-fold larger in human neurons (median 14 533 µm, first quartile 12 595 µm, third quartile 16 570 µm, $n = 60$) compared with mouse, *M. fascicularis* or *M. mulatta* neurons (mouse 5317 µm, $n = 15$; *M. fascicularis* 6248 µm, $n = 12$; *M. mulatta* 5239 µm, $n = 11$, all medians, $P < 0.0001$, Kruskal–Wallis, Fig. 6*C* and Table 2). Surprisingly, the macaque pyramidal neurons were more similar in dendritic length to mouse pyramidal neurons than to human pyramidal neurons. Considering the species-specific temporal cortical thickness (human 2773 µm, *M. fascicularis* 2300 µm (brainmaps.org), mouse 969 µm), total dendritic length apparently does not scale linearly to cortical thickness.

The measure "TDL" does not take into consideration that dendritic compartments can have very different functions (Spruston

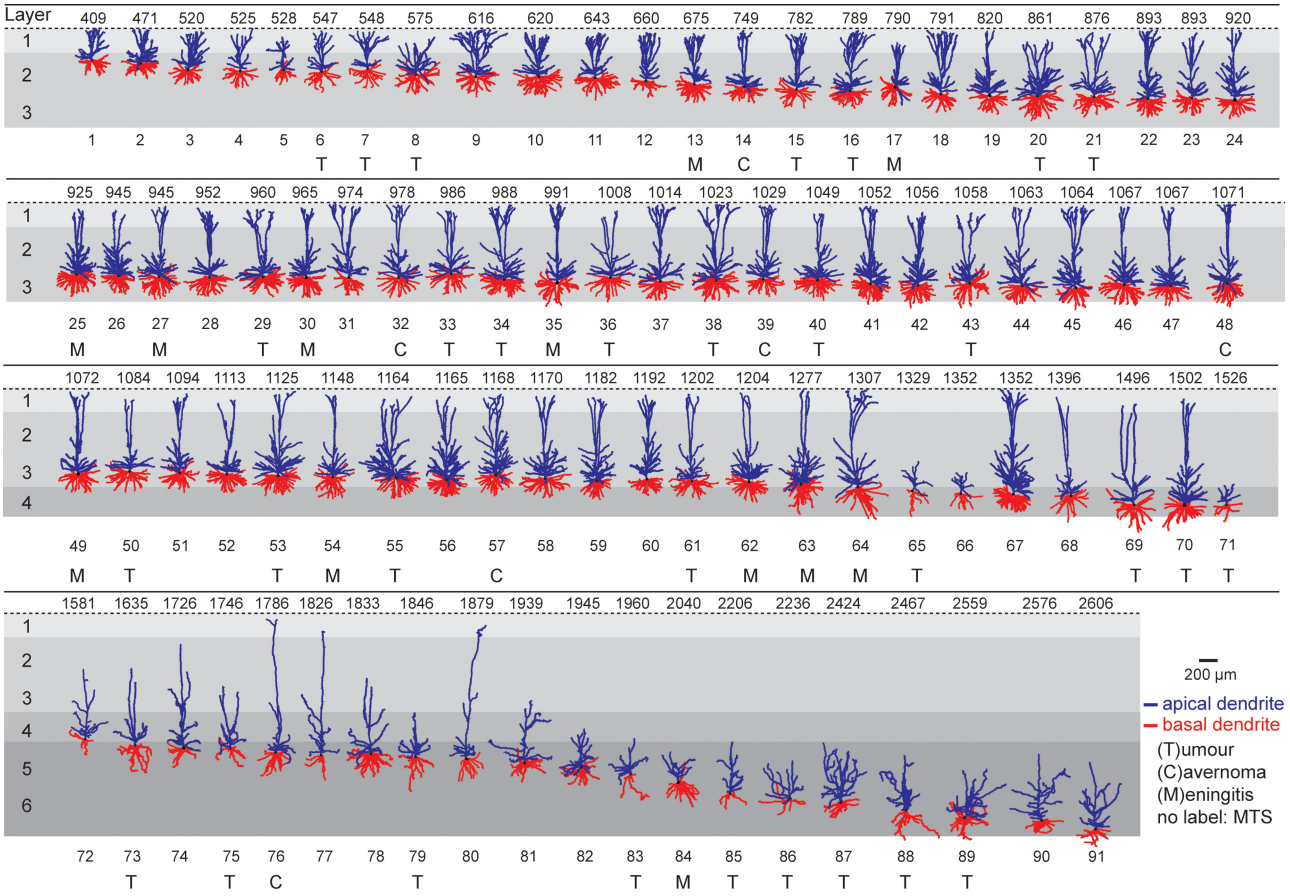

Figure 2. Dendrite gallery of human temporal cortex neurons. Representation of 91 3D reconstructed apical and basal dendrites of human temporal cortex (Brodmann area 21) arranged along somatic depth with respect to pial surface. Capitals (T, C, M) indicate that tissue was obtained from patients with subcortical tumor, cavarnoma, or meningitis. First row indicates depth in µm. Apical dendrite in blue, basal dendrite in red. Neurons not labeled originate from patients with mesiotemporal sclerosis (MTS).

2008; Larkum et al. 2009; Larkum 2013). Thus, we determined dendritic length for apical oblique dendrites, apical tuft, and basal dendrites separately (Fig. 6*D* and Table 2). The apical tuft was quantified as the dendritic length of all segments distal to the main bifurcation of the apical trunk with respect to the soma. The oblique dendrites were taken as the collection of branches originating from the main trunk, proximal to the main bifurcation of the apical trunk with respect to the soma. We found that all individual compartments (basal, main trunk, obliques, and tuft) showed larger dendritic length for human L2 and L3 neurons compared with mouse neurons (basal, oblique and tuft: $P < 0.0001$, Mann–Whitney, main trunk: $P < 0.01$, Mann–Whitney, Fig. 6*D* and Table 2).

Since branching pattern is a strong indicator of dendritic complexity (DeFelipe 2011), we compared the number of branch points between human and mouse neurons. The number of dendritic branch points per neuron was substantially different for basal and oblique dendrites, but not for the apical tuft in human neurons compared with mouse neurons (basal: $P < 0.01$, oblique: $P < 0.0001$, and tuft $P = 0.18$, Mann–Whitney, Fig. 6*E* Table 2).

Next, we determined whether these first-order structural parameters allow for unsupervised classification of human neurons from a pool of unlabeled morphologies. Since TDL and number of branch points were highly correlated (Fig. 6*F*), we only used TDL for cluster analysis. After randomized pooling of all available reconstructions from L2 and L3 temporal cortex of mouse, human, *M. fascicularis*, and *M. mulatta* ($n = 98$), unsupervised cluster analysis based on Euclidian distance and Thorndike procedure (Methods, (Thorndike 1953)) resulted in emergence of 2 major clusters with 53 of 60 human reconstructions isolated into one (red cluster, Fig. 6*G*). In contrast, neurons from mouse, *M. fascicularis* and *M. mulatta* clustered together and were thus virtually indistinguishable from each other (blue cluster, Fig. 6*G*). Based on TDL, 88% of human L2 and L3 neurons were thus classified into human-specific clusters and only 12% of human L2 and L3 neurons were comparable with neurons from mouse, *M. fascicularis* and *M. mulatta*. This shows that L2 and L3 pyramidal neurons in human temporal cortex have a distinct dendritic architecture compared with mouse, *M. fascicularis* and *M. mulatta*.

To quantify the differences in subcellular morphology between human and mouse neurons, we compared the segment length of both apical and basal dendrites using linear and quadratic polynomials in a MLM (Hox 2010). The segment length was determined as path length between branch points and we found that segment length increases significantly with distance from soma in both mouse and human neurons (Fig. 7*A–C*, $P < 0.01$ for both linear and quadratic effects, MLM). We also observed a significant difference in the rate of linear increase in segment length between human and mouse neurons (basal: $P < 0.001$, apical obliques: $P < 0.05$; and apical tuft $P < 0.001$, MLM). For basal and apical oblique dendrites, initial mouse and human segment lengths were comparable, but compared with mouse L2 and L3 temporal cortex neurons, human dendrites had significantly longer segments as from the third-, second-, and first-order segments

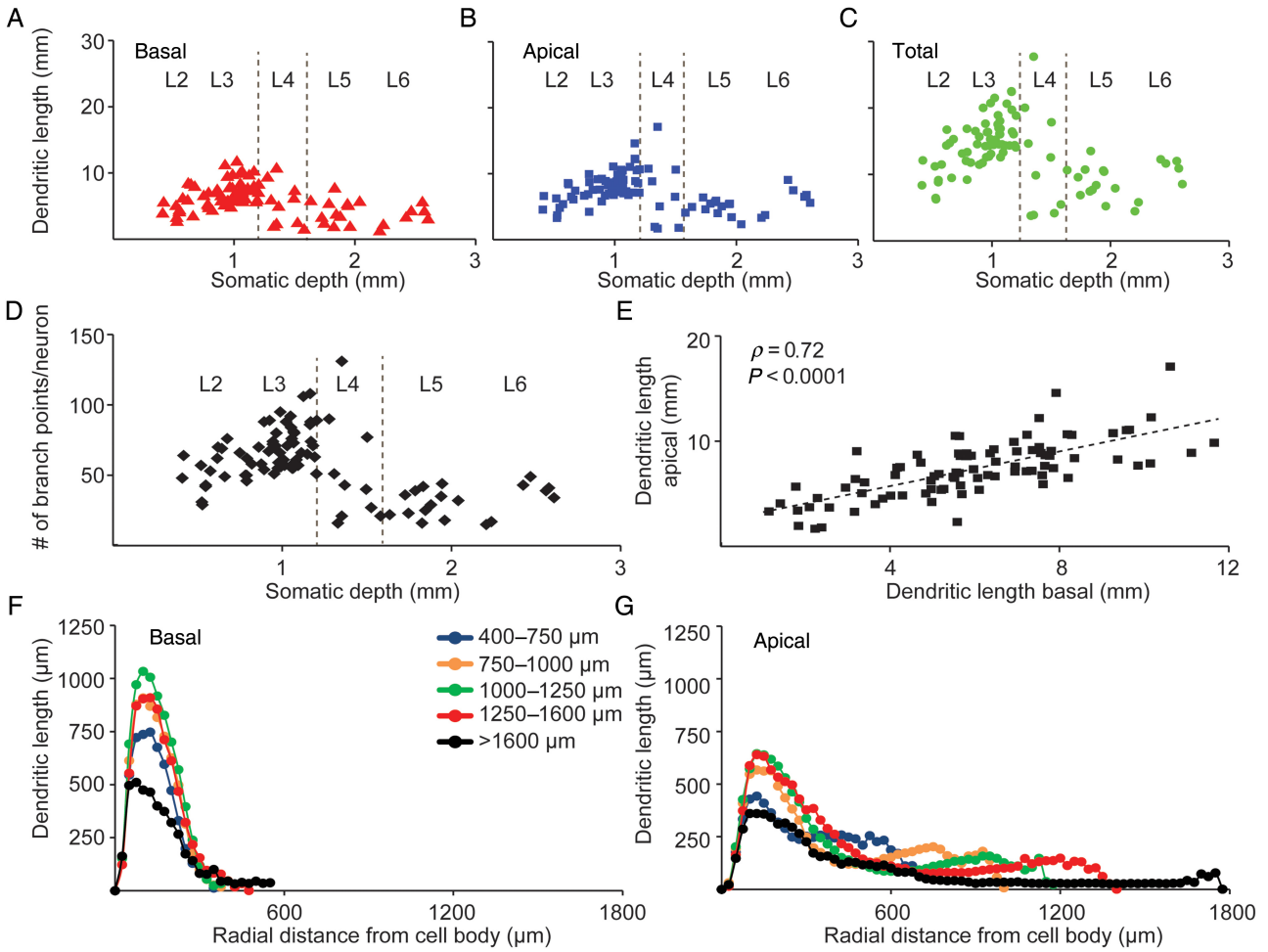

Figure 3. Layer-specific dendrite properties of human temporal cortex neurons. (*A*) Change in basal dendrite length of 91 human temporal cortex neurons with respect to layers and somatic depth. (*B*) Change in apical dendrite length with respect to layers and somatic depth. (*C*) Change in total dendrite length with respect to layers and somatic depth. (*D*) Change in number of branch points per neuron, for both apical and basal dendrites combined, with respect to layers and somatic depth. (*E*) Correlation between apical and basal dendrite length of 91 human temporal cortex neurons (Pearson's correlation coefficient $r = 0.71$, $P < 0.0001$). (*F*) Sholl analysis of 91 human temporal cortex basal dendrites, grouped into different depth bins, illustrating change in mean dendritic length with increasing radial distance from cell body. (*G*) Sholl analysis of apical dendrite with neurons grouped into different depth bins illustrating change in mean dendritic length with increasing radial distance from cell body.

of basal, apical oblique-, and apical tuft dendrites, respectively (Fig. 7A–C, $P < 0.001$, MLM). This shows that human pyramidal neurons are not linearly scaled with respect to mouse pyramidal neurons and scaling is compartment-specific.

Cortical pyramidal neurons in rodents have active electrical properties that facilitate electrical communication between the cell body and remote locations on distal dendrites (Larkum et al. 1999). We have found previously that larger dendrites have a strong impact on electrical behavior of neurons (Eyal et al. 2014). At present, little is known on active properties of human pyramidal neuron dendrites, what the properties are or whether basic membrane properties of human neurons are comparable with values reported in rodents (membrane capacitance or axial resistance). However, dendritic size, branch points, and dendrite thickness strongly determine the passive electrical properties of dendrites. To determine how subcellular dendritic architecture of human and mouse neurons affects passive electrical properties of dendrites, we used a detailed computational model. For both mouse and human populations, we took the most representative morphology (median TDL for the population; cell #44 for human). The study of the effect of dendritic architecture on passive attenuation in L2 and L3 neurons was performed by using the same specific values for membrane (R_m) and axial (R_i) resistivity for reconstruction of the electrotonic dendrogram for both mouse and human neurons ($R_m = 15\,000$ Ωcm^2 and $R_i = 150$ Ωcm, Fig. 8B1,B2, (Sarid et al. 2007)). In addition to these specific parameters, passive attenuation in dendrites depends also on segment length, dendritic diameter (space constant $\left(\lambda = \sqrt{(R_m/R_i) \times (\text{diam}/4)}\right)$), as well as on the boundary conditions at the ends of this dendritic segment (Rall 1959). With all these factors incorporated into the computational model, human neurons show much longer electrotonic means compared with mouse (Fig. 8C1,C2) and thus represent the first bottom-up step of building an accurate computational model of human pyramidal neurons. Further, a direct consequence of extended and more ramified dendrites was that forward- and backward spread of electrical signals showed larger attenuation in human compared with mouse (Fig. 8C–E). More specifically,

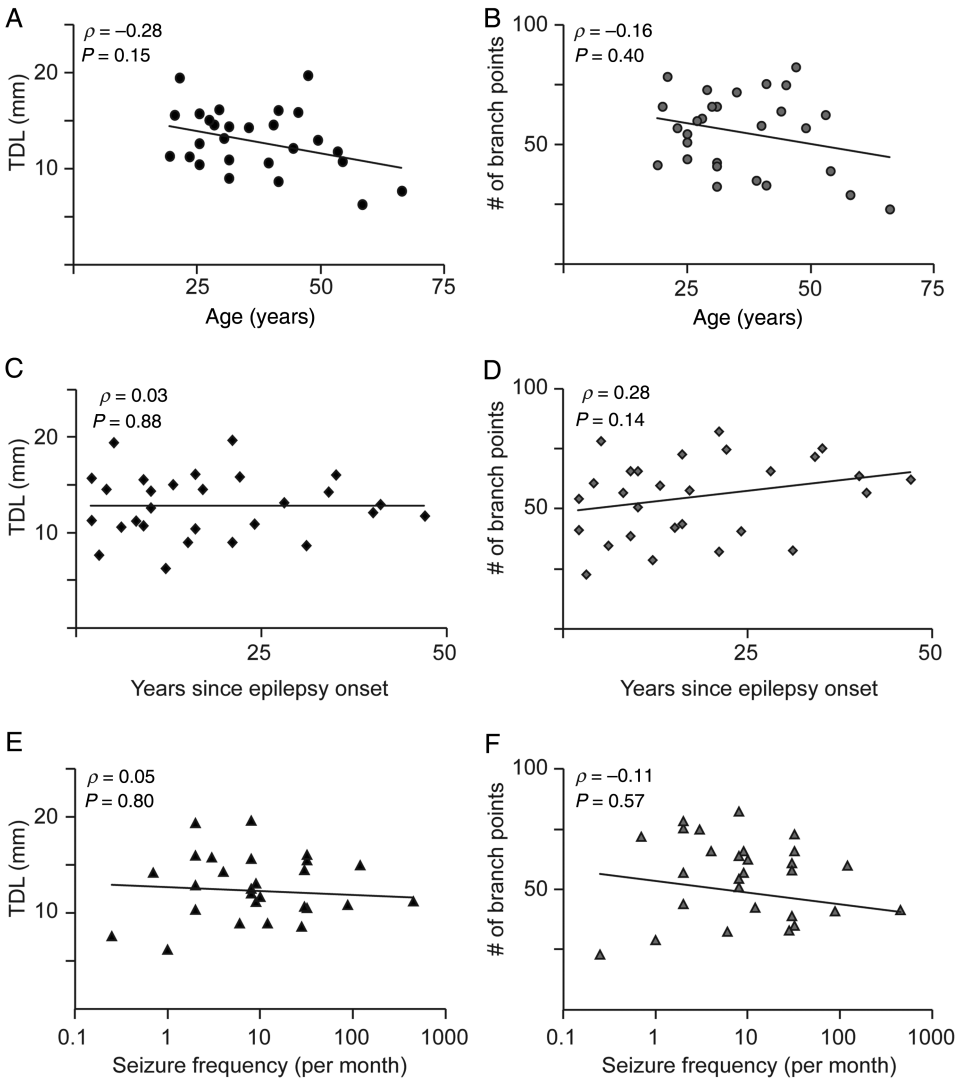

Figure 4. Disease history does not affect total dendritic length and number of branch points. (*A*) Correlation of total dendritic length with respect to age. Each point in the scatterplot represents the median value for a single patient (*B*) Correlation of number of branch points versus age. (*C*,*D*) Correlation for TDL and number of branch points, respectively, to years since epilepsy onset. (*E*,*F*) Correlation for TDL and number of branch points, respectively, to seizure frequency. Spearman's ρ and *P*-value are indicated within figure panels, respectively.

when comparing the soma voltage response for steady current injected at the dendrites (normalized to the soma response for somatic current injection), we found an average of 1.5-fold increase in the dendritic-to-soma (forward) voltage attenuation factor for the human versus the mouse L2 and L3 neuron (Fig. 8*C1*,*C2*). Steady-state voltage attenuation from dendrites to soma (taking into account local dendritic responses to current injections) shows a 2.5-fold increase in the average attenuation factor for the human versus the mouse neuron (Fig. 8*D1*,*D2*). Finally, backward propagating (from soma-to-dendrites) signals following steady-state current injection into the soma was also characterized by higher attenuation factor in the human neuron compared with mouse neuron (Fig. 8*E1*,*E2*). Active conductance mechanisms to propagate signals have been well documented in rodents, but we aimed at studying the direct effect of dendritic architecture on signal conduction. In addition, the vast array of potential active mechanisms that a neuron adopts to conduct signals would directly or indirectly depend on the inherent passive properties associated with its dendritic structure. Thus, the cellular architecture directly impacts passive electrical properties and behavior of human neurons, and affects both forward- and backward spread of electrical signals in dendrites.

Discussion

The human neocortex contains cell types that are not represented in the rodent neocortex (Nimchinsky et al. 1999; Oberheim et al. 2009; Radonjic et al. 2014). In this study, we asked the question whether the most abundant cell type of both human, rodent, and macaque neocortex, the pyramidal neurons, are morphologically similar or distinct in human, mouse, and macaque temporal cortex. Thereto, we made for the first time quantitative full 3D reconstructions of dendritic (basal/apical) and axonal architecture of adult human neurons of the temporal cortex. Because L2 and L3 holds a relatively homogenous class of pyramidal neurons, in contrast to deeper cortical layers (Arimatsu et al. 2003; Andjelic et al. 2009; Groh et al. 2010; Marx and Feldmeyer 2013; Bortone et al. 2014; Harris and Shepherd 2015), we restricted our study to L2 and L3 pyramidal neurons. By directly comparing

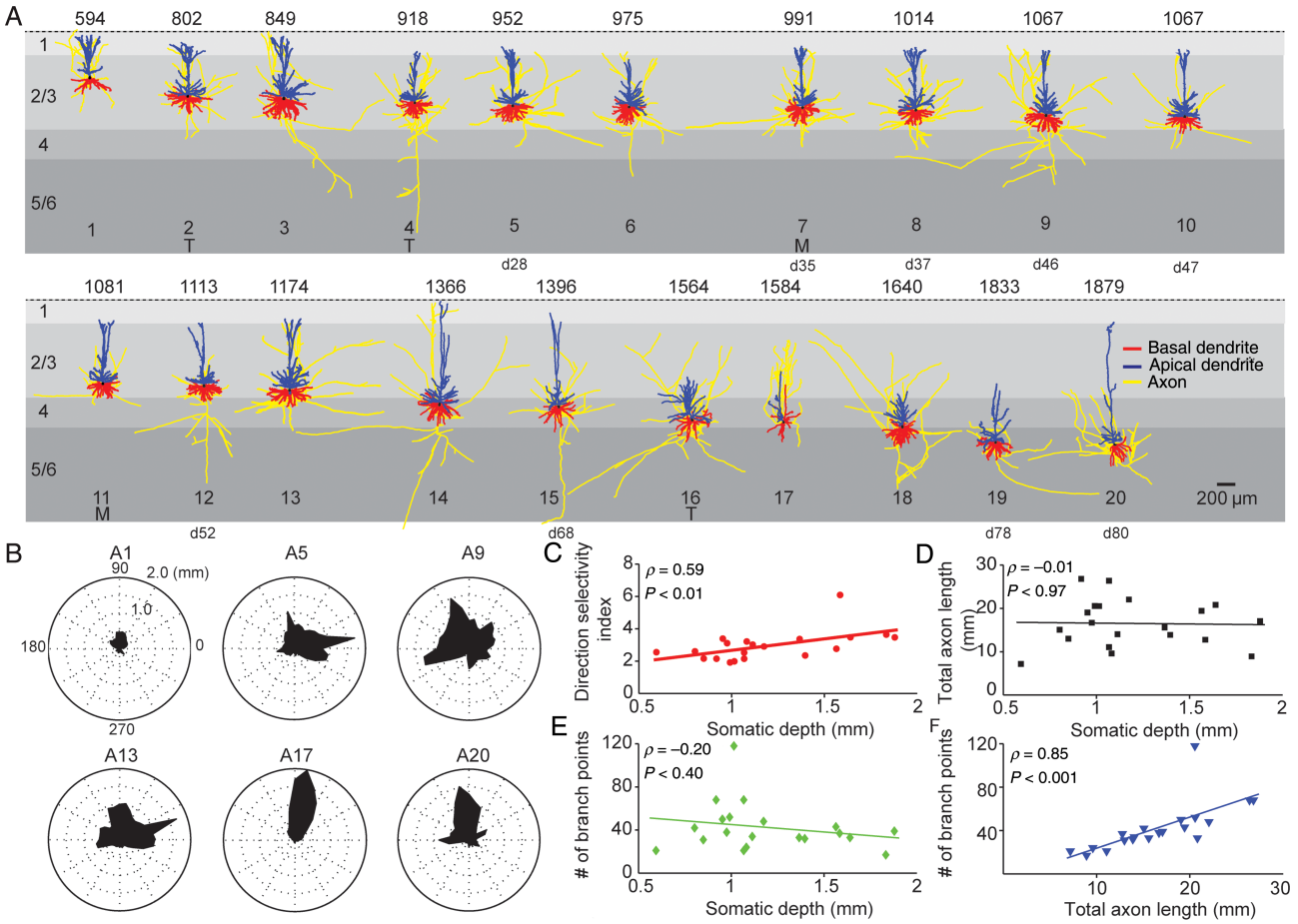

Figure 5. Axon gallery and layer-specific axonal properties of human temporal cortex neurons. (*A*) Representation of 20 3D reconstructed axons with apical and basal dendrites of human temporal cortex neurons arranged with respect to somatic depth. First row indicates somatic depth in µm. Last row indicates ID of the same reconstruction in dendrite gallery if present in both. Axons in yellow, apical dendrites in blue, basal dendrites in red. Capitals (T, M) indicate that tissue was obtained from patients with subcortical tumor or meningitis. Neurons that are also present in the dendrite gallery are indicated by cell number (for instance, cell #5 in axon gallery is cell 28 in dendrite gallery). (*B*) Polar plots of 6 example axonal reconstructions illustrating radial orientation of axons with respect to cell body. Top row indicates ID within axon gallery. (*C*) Dependence of direction selectivity index of axons with respect of somatic depth. (*D*) Dependence of total axon length with respect to depth. (*E*) Dependence of number of axonal branch points with respect to depth. (*F*) Correlation between total axonal length and number of axonal branch points.

with temporal cortex L2 and L3 pyramidal neurons of adult mice and macaque monkeys, we find that basic structural properties such as dendritic length, the number of branch points and segment length are different in human neurons. Human L2 and L3 pyramidal neurons have 3 times more dendrite than their mouse and macaque counterparts. Both basal dendrites and apical oblique dendrites (but not apical tuft) have more segments and, in particular, the distal segments are substantially longer in human pyramidal neurons. Cluster analysis showed that the majority of human L2 and L3 pyramidal neurons are morphologically distinct from mouse and macaque L2 and L3 pyramidal neurons.

Several studies have made direct comparisons of molecular, laminar, developmental, and cellular morphology between rodents, monkeys, and humans (Elston et al. 2001, 2011; Johnson et al. 2009; DeFelipe 2011; Kwan et al. 2012; Zeng et al. 2012). These studies highlight that complexity of neurons and astrocytes is substantially larger in human prefrontal and temporal cortex (Elston et al. 2001; DeFelipe et al. 2002; Oberheim et al. 2009). DeFelipe et al. (2002) reported that also other subcellular neuronal features, such as the shape of dendritic spines, the number of excitatory and inhibitory synapses received by neurons, as well as cell densities can differ substantially between human and rodent neocortex. From these studies, it is estimated that a human L2/L3 pyramidal neuron receives more than 30 000 synapses, approximately twice as much as is received by rodent L2/L3 pyramidal neurons (DeFelipe 2011). We found that human L2/L3 pyramidal neurons have 3 times more dendrite. This large dendritic tree can well accommodate a doubling of the number of input synapses.

Caveats of Human Tissue

In this study, we used brain tissue from 28 patients that underwent surgical treatment. This is brain tissue that is not part of the disease, but had to be removed to gain access to deeper brain structures for surgical treatment. In addition, we used temporal cortex tissue derived from different, unrelated types of patients, to test whether potential caveats due to secondary pathological effects of the disease mechanisms affected neuronal morphology. We found no systematic differences in dendrite morphology between neurons obtained from MTS, hippocampal tumor, meningitis, lesion, and cavernoma patients. More importantly, we also did not find any correlation between morphology

Table 2 Quantitative parameters of L2 and L3 neuronal complexity across species

Species	Total dendritic length (µm)	Length basal (µm)	Length apical (µm)	Length apical main trunk	Length apical obliques	Length apical tuft	# of branch points basal	# of branch points obliques	# of branch points tuft
M. fascicularis ($n = 12$)	**6247.87** 5140.39 7323.71	NA	NA	NA	NA	NA	NA	NA	NA
M. mulatta ($n = 11$)	**5238.59** 4760.04 5602.28	NA	NA	NA	NA	NA	NA	NA	NA
Human ($n = 60$)	**14533.00** 12594.98 16569.68	**6466.25** 5559.25 7695.30	**8005.90** 6775.42 8931.62	**209.20** 116.75 358.35	**4120.90** 2697.55 5064.25	**3642.95** 2438.38 4630.43	**31** 27 38	**13** 8 17	**12** 7 15
Mouse ($n = 15$)	**5316.80** 4904.15 6546.00	**3034.70** 2450.92 3681.55	**2512.00** 1991.30 3110.70	**34.70** 22.70 215.90	**512.00** 49.55 1215.65	**1580.10** 1332.75 2361.35	**22** 18 29	**2** 0 4	**13** 11 17

Note: Median values in bold, first and third quartile listed below, respectively. NA, not available.

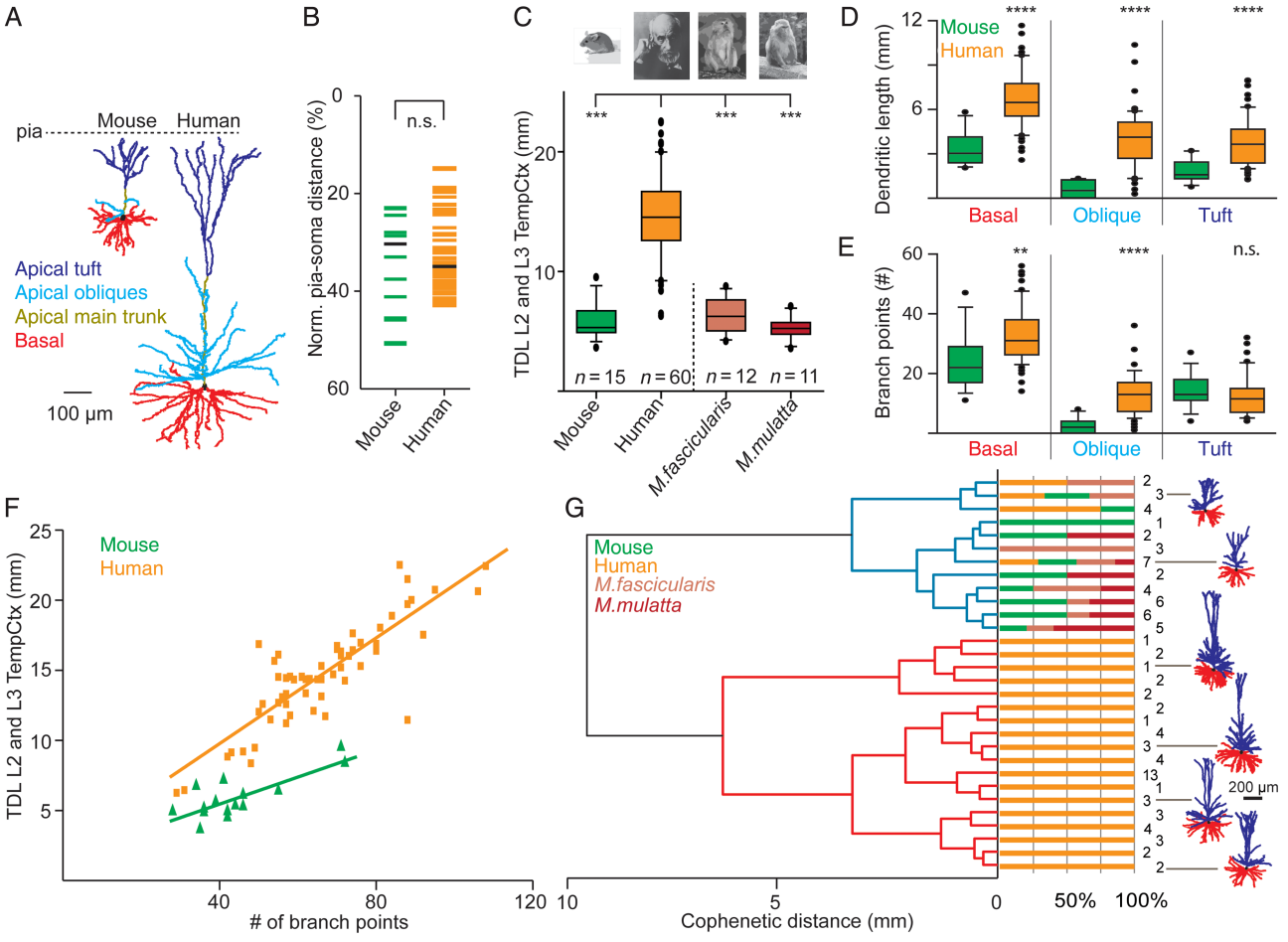

Figure 6. Comparison of dendritic complexity in human, monkey, and mouse L2 and L3 temporal cortex neurons. (*A*) Representative example 3D dendritic reconstructions of one mouse and human temporal cortex neuron. Apical main trunk in dark yellow, apical oblique dendrites in light blue, apical tuft in dark blue, basal dendrites in red, respectively. (*B*) Normalized pia-soma depth of individual L2 and L3 neurons from mouse and human temporal cortex. (*C*) Comparison of total dendritic length (TDL) between L2 and L3 temporal cortex neurons of mouse, human, *M. fascicularis*, and *M. mulatta*. (*D*) Comparison of basal, apical oblique, and apical tuft length between mouse and human temporal cortex neurons. (*E*) Number of branch points for mouse and human L2 and L3 temporal cortex neurons for basal, apical oblique, and apical tuft. (*F*) Correlation between number of branch points and TDL of human and mouse L2 and L3 temporal cortex neurons. (*G*) Dendrogram based on hierarchical agglomerative clustering of mouse, human, *M. fascicularis*, and *M. mulatta* L2 and L3 temporal cortex neurons. Neurons were grouped into 2 clusters indicated by blue and red dendrograms based on TDL. Note isolation of 88% of human neurons into unique red cluster.

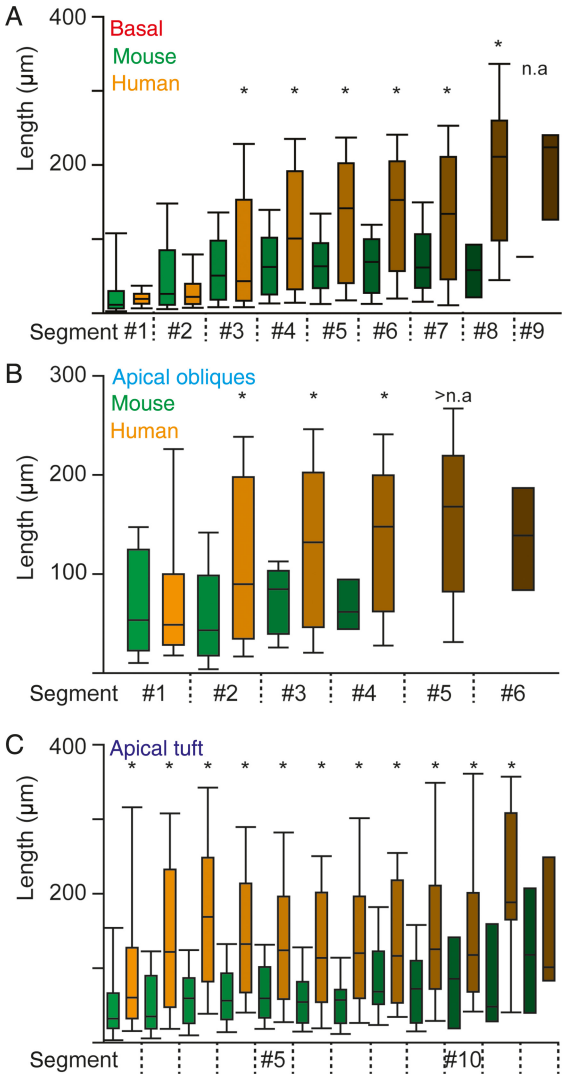

Figure 7. Elongated segments of basal, apical oblique and apical tuft dendrites in human neurons (*A*) Change in segment length of basal dendrites with distance from the soma of L2 and L3 neurons. Asterisks indicate statistical difference for human versus mouse (MLM statistics, see Materials and Methods) (*B*) Analogous to *A* for apical oblique dendrites. (*C*) Analogous to *A* for apical tuft dendrites.

(TDL and # of branch points) and disease etiology, disease duration since onset, disease intensity (# of seizures per month), and disease severity (total number of seizures) (Fig. 4). Since more elongated and more complex dendritic morphology of human temporal cortex neurons was consistent across patient populations, this is most likely not the result of a specific disease history. The only alternative method for studying the cellular organization of human brain is to obtain human tissue from postmortem brain. This approach suffers from other shortcomings, such as a drop in spine and dendrite densities that is observed already 1.5 h postmortem (de Ruiter and Uylings 1987; Swaab and Uylings 1988; Oberheim et al. 2009). Preliminary observations comparing basal dendrites of human temporal cortex L2 and L3 pyramidal neurons in surgical resection tissue and postmortem tissue showed that pyramidal neurons in postmortem tissue had 30% less basal dendrite length (Guy Eyal, Idan Segev, unpublished observations). The outcome of this specific comparison could be due to ischemia-induced neurotoxic processes in the time delay from death to brain fixation, or to differences in the age of subjects used which was higher for the postmortem brain tissue. The average age of patients in our study was 36.0 ± 12.4 years. One of the strengths of our approach is that the comparison between human and mouse pyramidal neurons was done using the exact same methods of single neuron labeling in acute, living brain slices of adult temporal cortex in the same laboratory.

Important to note however is that standardization protocols for rodent brain research are much more advanced compared with human brain research. Increasingly difficult to control for in human brain research are genetic and nongenetic factors that could contribute to neuronal morphology. The genetic background of the human population is highly diverse and nongenetic factors influencing fine-scale cortical organization are not controlled for. For instance, presurgical medication with antiepileptic drugs is highly subject-specific (Table 1) and lifetime use of alcohol, nicotine, or caffeine is largely unknown. It seems highly unlikely though that those genetic and environmental factors could have such a consistent and profound effect on cellular morphology explaining the 3-fold difference in TDL between mouse and human. Future studies and increasing information on subcellular organization of human brain will be the only framework in which the interdependence between neuronal morphology in human brain and genetic/environmental factors can be investigated.

Functional Consequences for Distal Synapses

With larger dendritic trees and more input synapses, human L2 and L3 pyramidal neurons seem to be larger integration centers compared with rodent L2 and L3 pyramidal neurons. Yet, larger dendrites and more branch points will mean that input synapses on distal segments run the risk of having little impact on the cell body membrane potential. Using computational modeling of the cable properties of L2 and L3 neurons, we showed that the morphological differences between mouse and human directly affect the electrical properties of dendrites. Both forward and backward propagation of electrical signals are affected and are strongly attenuated in human dendrites. This first step in computationally modeling the electrical behavior of human neurons may suggest that distal dendrites of human neurons can act electrically more independently from the soma. Alternatively, additional synaptic amplification or nonlinear dendritic mechanisms may exist in human dendrites that could aid dendritic propagation of electrical signals (Chen et al. 2011; Lavzin et al. 2012). We have recently shown that action potentials evoked at the soma of human temporal cortex neurons induce sharp calcium transients in the dendrite that can be blunted by L-type calcium channel blockers (Verhoog et al. 2013). How active human dendrites are and whether the distribution of dendritic voltage-dependent conductances resemble those in rodent pyramidal neurons (Larkum et al. 1999), awaits direct dendritic recordings.

Functional Consequences for Action Potential Output

Does a 3 times larger dendritic tree have functional consequences for the output of neurons, that is, action potential firing and encoding properties of neurons? Recently, we found that there is a profound functional cross-talk between the dendritic tree and the axon initial segment that depends on the passive electrical properties of dendrites (Eyal et al. 2014). The cable properties of the dendritic tree, which follow from the morphological features, directly affect the shape of action potential onset at the axon initial segment: the larger the dendritic tree is relative to the

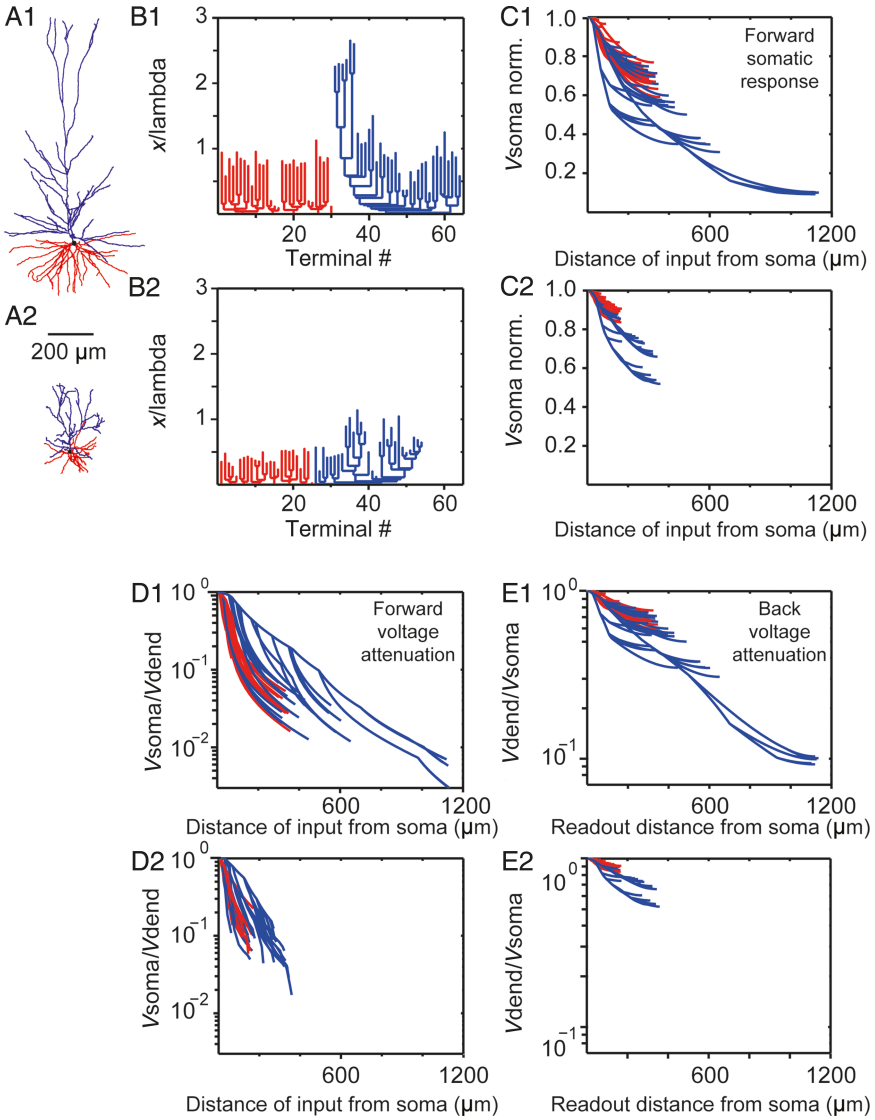

Figure 8. Electrotonic structure and voltage attenuation in human versus mouse L2 and L3 pyramidal cells. (*A1*, *A2*) Morphology of human and mouse temporal cortex example neurons, respectively. Red denotes basal tree whereas blue the apical tree, respectively. (*B1*, *B2*) Dendrogram in cable units for the neurons in *A1* and *A2*, respectively. In both cases, $R_m = 15\,000\ \Omega cm^2$ and $R_i = 150\ \Omega cm$. (*C1*, *C2*) Normalized soma voltage resulting from steady-state current injection in the corresponding dendritic sites for the example neurons in *A1*, *A2*, respectively. Each line represents a path from the soma to a dendritic terminal. Note the 1.5-fold increase in the average voltage attenuation for the human versus the mouse cell and the enhance attenuation from the distal apical tuft in the human neuron. (*D1*, *D2*) Steady voltage attenuation from the dendrites (V_{dend}) to the soma (V_{soma}) for the neurons in *A1*, *A2*, respectively. Note the 2.5-fold increase in the average attenuation for the human versus the mouse neuron. (*E1*, *E2*) Steady-state voltage attenuation from the soma to the dendrites for the neurons in *A1*, *A2*, respectively.

axon initial segment, that is, the larger the conductance load of the dendritic tree is on the axon initial segment, the faster the action potential onset. Experimentally manipulating the size of the dendritic tree has directly demonstrated that the shape of the action potential onset depends on the dendritic load (Bekkers and Hausser 2007). Therefore, we expect that human L2 and L3 temporal cortex pyramidal neurons have a faster action potential onset than those of the mouse. We recently tested this hypothesis and indeed found that action potentials of human L2 and L3 pyramidal neurons have faster onset kinetics (Testa-Silva et al. 2014). In particular when neurons repeatedly fired once per second or more, the action potential onset of human pyramidal neurons was substantially faster than mouse pyramidal neurons.

Fourcaud-Trocme et al. (2003) showed that fast action potential onset dynamics endows neurons with the ability to time action potentials relative to fast subthreshold membrane potential changes. Thereby, action potentials can be phase-locked to fast synaptic inputs. The reason for this can be intuitively understood: a steep action potential enables the axon to respond fast to rapid membrane potential changes, whereas a less steep action potential onset will not be fast enough and, in the extreme case, it will "ignore" the underlying voltage modulations. In that case, neurons will fire action potentials at arbitrary time points with respect to fast synaptic inputs. Because of the effect of dendritic cable properties on action potential onset, which determines the encoding capability of neurons (Fourcaud-Trocme et al. 2003; Ilin et al. 2013), we predicted that neurons with large dendritic trees, such as human L2 and L3 pyramidal neurons, have an improved capability for rapid timing of action potentials and thereby encoding of fast synaptic inputs by axonal action

potentials (Eyal et al. 2014). We recently indeed found that human L2 and L3 temporal cortex pyramidal neurons can much better encode rapid membrane potential changes with submillisecond time resolution in action potential timing than mouse L2 and L3 pyramidal neurons can (Testa-Silva et al. 2014). We now show here that human L2 and L3 pyramidal neurons actually have a 3 times larger dendritic tree than mouse pyramidal neurons. Together with the effect of dendritic tree size on action potential kinetics, we conclude that the larger dendrites of human L2 and L3 pyramidal neurons can explain both the faster action potential onset and encoding of faster membrane potential changes in action potential timing with respect to mouse pyramidal neurons (Eyal et al. 2014; Testa-Silva et al. 2014). It will be interesting to learn whether action potential onset dynamics and synaptic input tracking capabilities of macaque L2 and L3 pyramidal neurons are similar to those of mouse pyramidal neurons, as are their dendritic trees. Possibly, the extended dendritic morphology of cortical pyramidal neurons and the faster physiology of these neurons provide a cellular substrate for many of the distinct cognitive capabilities of humans.

Funding

S.v.d.S. is financially supported by the Netherlands Scientific Organization (NWO/MaGW: VIDI-452-12-014). Part of this project was supported by Hersenstichting Nederland (grant HSN 2010(1)-09 to C.P.J.d.K.), Center for Neurogenomics and Cognitive Research (CNCR), Neuroscience Campus Amsterdam (NCA), VU University Amsterdam and by the Human Brain Project (to I.S.). H.M. is a recipient of an Erasmus Mundus Joint Doctorate grant (ENC-Network). K.K.D. and J.O. are funded by EU MSCA-ITN CognitionNet (FP7-PEOPLE-2013-ITN 607508). H.D.M. received funding for this work from the Netherlands Organization for Scientific Research (NWO; 917.76.360, 912.06.148, and a VICI grant), ERC StG "Brain-Signals," the Dutch Fund for Economic Structure Reinforcement (FES, 0908 "NeuroBasic PharmaPhenomics project"), EU 7th Framework Programmes (HEALTH-F2-2009-242167 "SynSys" and grant agreement no. 604102 "Human Brain Project"). Funding to pay the Open Access publication charges for this article was provided by the Center for Neurogenomics and Cognitive Research (CNCR), VU University Amsterdam.

Notes

We are grateful for the individuals that donated their cortical tissue to our study. We also thank Fritjof Helmchen and Randy Bruno for valuable comments on a previous version of this manuscript, Marcel Oberlaender, Robert Egger, Andrew Johnson, Simon-Shlomo Poil, Klaus Linkenkaer-Hansen, Albert Gidon, Chayada Chotsiruparat, and Barbara Kits for fruitful collaborations and analyses at early stages of this project. We also thank Hans Lodder, Jasper Stroeder, Rogier Poorthuis, Rhiannon Meredith, and Martha Ruiperez Alonso for assistance during a subset of the experiments and Conor V. Dolan for statistical advice. *Conflict of Interest*: None declared.

References

Aarts E, Verhage M, Veenvliet JV, Dolan CV, van der Sluis S. 2014. A solution to dependency: using multilevel analysis to accommodate nested data. Nat Neurosci. 17:491–496.

Anderson K, Bones B, Robinson B, Hass C, Lee H, Ford K, Roberts TA, Jacobs B. 2009. The morphology of supragranular pyramidal neurons in the human insular cortex: a quantitative Golgi study. Cereb Cortex. 19:2131–2144.

Andjelic S, Gallopin T, Cauli B, Hill EL, Roux L, Badr S, Hu E, Tamas G, Lambolez B. 2009. Glutamatergic nonpyramidal neurons from neocortical layer VI and their comparison with pyramidal and spiny stellate neurons. J Neurophysiol. 101:641–654.

Arimatsu Y, Ishida M, Kaneko T, Ichinose S, Omori A. 2003. Organization and development of corticocortical associative neurons expressing the orphan nuclear receptor Nurr1. J Comp Neurol. 466:180–196.

Ascoli GA. 2006. Mobilizing the base of neuroscience data: the case of neuronal morphologies. Nat Rev Neurosci. 7:318–324.

Bekkers JM, Hausser M. 2007. Targeted dendrotomy reveals active and passive contributions of the dendritic tree to synaptic integration and neuronal output. Proc. Natl Acad. Sci. USA. 104:11447–11452.

Bianchi S, Stimpson CD, Bauernfeind AL, Schapiro SJ, Baze WB, McArthur MJ, Bronson E, Hopkins WD, Semendeferi K, Jacobs B, et al. 2013. Dendritic morphology of pyramidal neurons in the chimpanzee neocortex: regional specializations and comparison to humans. Cereb Cortex. 23:2429–2436.

Bortone DS, Olsen SR, Scanziani M. 2014. Translaminar inhibitory cells recruited by layer 6 corticothalamic neurons suppress visual cortex. Neuron. 82:474–485.

Braak H. 1980. Architectonics of the human telencephalic cortex. Berlin, Heidelberg: Springer.

Bruno RM, Hahn TT, Wallace DJ, de Kock CP, Sakmann B. 2009. Sensory experience alters specific branches of individual corticocortical axons during development. J Neurosci. 29:3172–3181.

Carnevale NT, Hines ML. 2006. The NEURON book. Cambridge (UK): Cambridge University Press.

Chen X, Leischner U, Rochefort NL, Nelken I, Konnerth A. 2011. Functional mapping of single spines in cortical neurons in vivo. Nature. 475:501–505.

Clowry G, Molnar Z, Rakic P. 2010. Renewed focus on the developing human neocortex. J Anat. 217:276–288.

Cuntz H, Forstner F, Borst A, Hausser M. 2010. One rule to grow them all: a general theory of neuronal branching and its practical application. PLoS Comput Biol. 6(8):1–14.

DeFelipe J. 2011. The evolution of the brain, the human nature of cortical circuits, and intellectual creativity. Front Neuroanat. 5:29.

DeFelipe J, Alonso-Nanclares L, Arellano JI. 2002. Microstructure of the neocortex: comparative aspects. Journal of Neurocytology. 31:299–316.

de Ruiter JP, Uylings HB. 1987. Morphometric and dendritic analysis of fascia dentata granule cells in human aging and senile dementia. Brain Res. 402:217–229.

Duan H, Wearne SL, Morrison JH, Hof PR. 2002. Quantitative analysis of the dendritic morphology of corticocortical projection neurons in the macaque monkey association cortex. Neuroscience. 114:349–359.

Duan H, Wearne SL, Rocher AB, Macedo A, Morrison JH, Hof PR. 2003. Age-related dendritic and spine changes in corticocortically projecting neurons in macaque monkeys. Cereb Cortex. 13:950–961.

Dzaja D, Hladnik A, Bicanic I, Bakovic M, Petanjek Z. 2014. Neocortical calretinin neurons in primates: increase in proportion and microcircuitry structure. Front Neuroanat. 8:103.

Egger V, Nevian T, Bruno RM. 2008. Subcolumnar dendritic and axonal organization of spiny stellate and star pyramid

neurons within a barrel in rat somatosensory cortex. Cereb Cortex. 18:876–889.
Elston GN, Benavides-Piccione R, DeFelipe J. 2001. The pyramidal cell in cognition: a comparative study in human and monkey. J Neurosci. 21:RC163.
Elston GN, Benavides-Piccione R, Elston A, Manger PR, DeFelipe J. 2011. Pyramidal cells in prefrontal cortex of primates: marked differences in neuronal structure among species. Front Neuroanat. 5:2.
Eyal G, Mansvelder HD, de Kock CP, Segev I. 2014. Dendrites impact the encoding capabilities of the axon. J Neurosci. 34:8063–8071.
Fischl B, Dale AM. 2000. Measuring the thickness of the human cerebral cortex from magnetic resonance images. Proc Natl Acad Sci USA. 97:11050–11055.
Fourcaud-Trocme N, Hansel D, van Vreeswijk C, Brunel N. 2003. How spike generation mechanisms determine the neuronal response to fluctuating inputs. J Neurosci. 23: 11628–11640.
Geschwind DH, Rakic P. 2013. Cortical evolution: judge the brain by its cover. Neuron. 80:633–647.
Groh A, Meyer HS, Schmidt EF, Heintz N, Sakmann B, Krieger P. 2010. Cell-type specific properties of pyramidal neurons in neocortex underlying a layout that is modifiable depending on the cortical area. Cereb Cortex. 20:826–836.
Harris KD, Shepherd GM. 2015. The neocortical circuit: themes and variations. Nat Neurosci. 18:170–181.
Hladnik A, Dzaja D, Darmopil S, Jovanov-Milosevic N, Petanjek Z. 2014. Spatio-temporal extension in site of origin for cortical calretinin neurons in primates. Front Neuroanat. 8:50.
Horikawa K, Armstrong WE. 1988. A versatile means of intracellular labeling: injection of biocytin and its detection with avidin conjugates. J Neurosci Methods. 25:1–11.
Hox JJ. 2010. Multilevel analysis: techniques and applications. New Jersey: Erlbaum.
Ilin V, Malyshev A, Wolf F, Volgushev M. 2013. Fast computations in cortical ensembles require rapid initiation of action potentials. J Neurosci. 33:2281–2292.
Jacobs B, Driscoll L, Schall M. 1997. Life-span dendritic and spine changes in areas 10 and 18 of human cortex: a quantitative Golgi study. J Comp Neurol. 386:661–680.
Jacobs B, Schall M, Prather M, Kapler E, Driscoll L, Baca S, Jacobs J, Ford K, Wainwright M, Treml M. 2001. Regional dendritic and spine variation in human cerebral cortex: a quantitative golgi study. Cereb Cortex. 11:558–571.
Johnson MB, Kawasawa YI, Mason CE, Krsnik Z, Coppola G, Bogdanovic D, Geschwind DH, Mane SM, State MW, Sestan N. 2009. Functional and evolutionary insights into human brain development through global transcriptome analysis. Neuron. 62:494–509.
Kwan KY, Lam MM, Johnson MB, Dube U, Shim S, Rasin MR, Sousa AM, Fertuzinhos S, Chen JG, Arellano JI, et al. 2012. Species-dependent posttranscriptional regulation of NOS1 by FMRP in the developing cerebral cortex. Cell. 149:899–911.
Larkum M. 2013. A cellular mechanism for cortical associations: an organizing principle for the cerebral cortex. Trends Neurosci. 36:141–151.
Larkum ME, Kaiser KM, Sakmann B. 1999. Calcium electrogenesis in distal apical dendrites of layer 5 pyramidal cells at a critical frequency of back-propagating action potentials. Proc. Natl Acad. Sci. USA. 96:14600–14604.
Larkum ME, Nevian T, Sandler M, Polsky A, Schiller J. 2009. Synaptic integration in tuft dendrites of layer 5 pyramidal neurons: a new unifying principle. Science. 325:756–760.
Lavzin M, Rapoport S, Polsky A, Garion L, Schiller J. 2012. Nonlinear dendritic processing determines angular tuning of barrel cortex neurons in vivo. Nature. 490:397–401.
Luebke JI, Medalla M, Amatrudo JM, Weaver CM, Crimins JL, Hunt B, Hof PR, Peters A. 2015. Age-related changes to layer 3 pyramidal cells in the rhesus monkey visual cortex. Cereb Cortex. 25:1454–1468.
Magee JC. 2000. Dendritic integration of excitatory synaptic input. Nat Rev Neurosci. 1:181–190.
Mainen ZF, Sejnowski TJ. 1996. Influence of dendritic structure on firing pattern in model neocortical neurons. Nature. 382: 363–366.
Marx M, Feldmeyer D. 2013. Morphology and physiology of excitatory neurons in layer 6b of the somatosensory rat barrel cortex. Cereb Cortex. 23:2803–2817.
Morales J, Benavides-Piccione R, Dar M, Fernaud I, Rodriguez A, Anton-Sanchez L, Bielza C, Larranaga P, DeFelipe J, Yuste R. 2014. Random positions of dendritic spines in human cerebral cortex. J Neurosci. 34:10078–10084.
Narayanan RT, Egger R, Johnson AS, Mansvelder HD, Sakmann B, de Kock CPJ, Oberlaender M. 2015. Beyond columnar organization: cell type- and target layer-specific principles of horizontal axon projection patterns in rat vibrissal cortex. Cereb Cortex. 25:4450–4468.
Neuromorpho.org. http://neuromorpho.org/neuroMorpho/index.jsp.
Nimchinsky EA, Gilissen E, Allman JM, Perl DP, Erwin JM, Hof PR. 1999. A neuronal morphologic type unique to humans and great apes. Proc Natl Acad Sci USA. 96:5268–5273.
Oberheim NA, Takano T, Han X, He W, Lin JH, Wang F, Xu Q, Wyatt JD, Pilcher W, Ojemann JG, et al. 2009. Uniquely hominid features of adult human astrocytes. J Neurosci. 29:3276–3287.
Oberlaender M, Boudewijns ZS, Kleele T, Mansvelder HD, Sakmann B, de Kock CP. 2011. Three-dimensional axon morphologies of individual layer 5 neurons indicate cell type-specific intracortical pathways for whisker motion and touch. Proc Natl Acad Sci USA. 108:4188–4193.
Ong WY, Garey LJ. 1990. Neuronal architecture of the human temporal cortex. Anat Embryol. 181:351–364.
Petanjek Z, Judas M, Kostovic I, Uylings HB. 2008. Lifespan alterations of basal dendritic trees of pyramidal neurons in the human prefrontal cortex: a layer-specific pattern. Cereb Cortex. 18:915–929.
Petanjek Z, Judas M, Simic G, Rasin MR, Uylings HB, Rakic P, Kostovic I. 2011. Extraordinary neoteny of synaptic spines in the human prefrontal cortex. Proc Natl Acad Sci USA. 108:13281–13286.
Radonjic NV, Ayoub AE, Memi F, Yu X, Maroof A, Jakovcevski I, Anderson SA, Rakic P, Zecevic N. 2014. Diversity of cortical interneurons in primates: the role of the dorsal proliferative niche. Cell Rep. 9:2139–2151.
Rakic P. 2009. Evolution of the neocortex: a perspective from developmental biology. Nat Rev Neurosci. 10:724–735.
Rall W. 1959. Branching dendritic trees and motoneuron membrane resistivity. Exp Neurol. 1:491–527.
Ravid R, Swaab DF. 1993. The Netherlands brain bank—a clinicopathological link in aging and dementia research. J Neural Transm Suppl. 39:143–153.
Rosoklija GB, Petrushevski VM, Stankov A, Dika A, Jakovski Z, Pavlovski G, Davcheva N, Lipkin R, Schnieder T, Scobie K, et al. 2014. Reliable and durable Golgi staining of brain tissue from human autopsies and experimental animals. J Neurosci Methods. 230:20–29.

Sarid L, Bruno R, Sakmann B, Segev I, Feldmeyer D. 2007. Modeling a layer 4-to-layer 2/3 module of a single column in rat neocortex: interweaving in vitro and in vivo experimental observations. Proc Natl Acad Sci USA. 104:16353–16358.

Segev I, Rall W. 1998. Excitable dendrites and spines: earlier theoretical insights elucidate recent direct observations. Trends Neurosci. 21:453–460.

Spruston N. 2008. Pyramidal neurons: dendritic structure and synaptic integration. Nat Rev Neurosci. 9:206–221.

Swaab DF, Uylings HBM. 1988. Potentialities and pitfalls in the use of human brain material in molecular neuroanatomy. In: van Leeuwen FW, Buijs RM, Pool CW, Pach O, editors. Molecular Neuroanatomy. Elsevier Science Publishers B.V. p. 403–416.

Testa-Silva G, Verhoog MB, Goriounova NA, Loebel A, Hjorth J, Baayen JC, de Kock CP, Mansvelder HD. 2010. Human synapses show a wide temporal window for spike-timing-dependent plasticity. Front Synapt Neurosci. 2:12.

Testa-Silva G, Verhoog MB, Linaro D, de Kock CP, Baayen JC, Meredith RM, De Zeeuw CI, Giugliano M, Mansvelder HD. 2014. High bandwidth synaptic communication and frequency tracking in human neocortex. PLoS Biol. 12: e1002007.

Thorndike RL. 1953. Who belongs in the family? Psychometrika. 18:10.

van Elburg RA, van Ooyen A. 2010. Impact of dendritic size and dendritic topology on burst firing in pyramidal cells. PLoS Comput Biol. 6:e1000781.

van Pelt J, van Ooyen A, Uylings HB. 2014. Axonal and dendritic density field estimation from incomplete single-slice neuronal reconstructions. Front Neuroanat. 8:54.

Verhoog MB, Goriounova NA, Obermayer J, Stroeder J, Hjorth JJ, Testa-Silva G, Baayen JC, de Kock CP, Meredith RM, Mansvelder HD. 2013. Mechanisms underlying the rules for associative plasticity at adult human neocortical synapses. J Neurosci. 33:17197–17208.

Yuste R, Tank DW. 1996. Dendritic integration in mammalian neurons, a century after Cajal. Neuron. 16:701–716.

Zeba M, Jovanov-Milosevic N, Petanjek Z. 2008. Quantitative analysis of basal dendritic tree of layer III pyramidal neurons in different areas of adult human frontal cortex. Coll Antropol. 32(Suppl 1):161–169.

Zeng H, Shen EH, Hohmann JG, Oh SW, Bernard A, Royall JJ, Glattfelder KJ, Sunkin SM, Morris JA, Guillozet-Bongaarts AL, et al. 2012. Large-scale cellular-resolution gene profiling in human neocortex reveals species-specific molecular signatures. Cell. 149:483–496.